# Journal of Materials Chemistry A

Accepted Manuscript


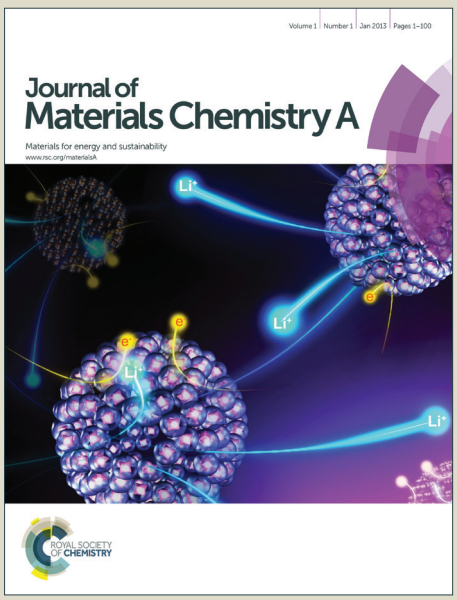



This is an *Accepted Manuscript*, which has been through the Royal Society of Chemistry peer review process and has been accepted for publication.

*Accepted Manuscripts* are published online shortly after acceptance, before technical editing, formatting and proof reading. Using this free service, authors can make their results available to the community, in citable form, before we publish the edited article. We will replace this *Accepted Manuscript* with the edited and formatted *Advance Article* as soon as it is available.

You can find more information about *Accepted Manuscripts* in the Information for Authors.

Please note that technical editing may introduce minor changes to the text and/or graphics, which may alter content. The journal's standard Terms & Conditions and the Ethical guidelines still apply. In no event shall the Royal Society of Chemistry be held responsible for any errors or omissions in this *Accepted Manuscript* or any consequences arising from the use of any information it contains.



ROYAL SOCIETY OF CHEMISTRY

www.rsc.org/materialsA

## Graphical Abstract

Shape controlled functionalized graphene/$MnO_2$ composites with high capacitive performance can be obtained by self-assembly.

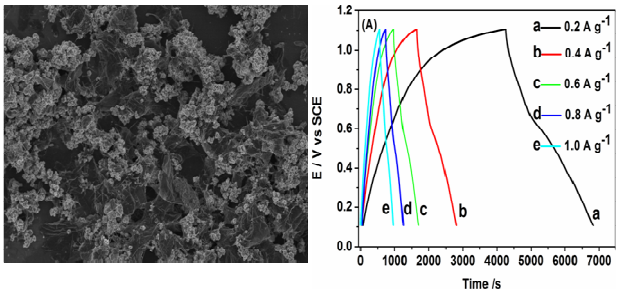


Journal of Materials Chemistry A Accepted Manuscript

# The Self-Assembly of Shape Controlled Functionalized Graphene/$MnO_2$ Composites for Supercapacitors

Xiaomiao Feng,*[1] Ningna Chen,[1] Yu Zhang, Zhenzhen Yan, Xingfen Liu, Yanwen Ma,* Qingming Shen, Lianhui Wang, Wei Huang

Key Laboratory for Organic Electronics & Information Displays, Institute of Advanced Materials, School of Materials Science & Engineering, Nanjing University of Posts and Telecommunications, Nanjing 210046, China.

E-mail: iamxmfeng@njupt.edu.cn; iamywma@njupt.edu.cn

1 These authors contributed equally to this work.

**Abstract:** Graphene/$MnO_2$ nanocomposites with different morphologies were obtained by a facile self-assembly method. The formation mechanism of graphene/$MnO_2$ composites with different shapes of $MnO_2$ were discussed in detail. Nanostructured $MnO_2$ with different morphologies was distributed on the surface of graphene uniformly. The prepared graphene/$MnO_2$ composites could be used for electrode materials of supercapacitors. The graphene/$MnO_2$ (flowerlike nanospheres) composite (405 F $g^{-1}$) exhibited better capacitive performances than that of the graphene/$MnO_2$ (nanowires) composite (318 F $g^{-1}$) at a current density of 1.0 A $g^{-1}$. The synergistic effect of graphene and $MnO_2$ endowed the composite with high electrochemical capacitance. Moreover, the graphene/$MnO_2$ (flowerlike nanospheres) composite showed fast charge-discharge process and high cyclic stability.

**Key Words:** Graphene, $MnO_2$, self-assembly, supercapacitors

## 1. Introduction

In the past years, electrochemical supercapacitors (ECs) have raised much attention in the field of applied electrochemical energy conservation/storage systems. Supercapacitors, which are also called ultracapacitors, are electricity storage device between conventional capacitors and rechargeable batteries. They have a wide application in electric vehicles, portable electronic devices, memory back-up devices, large industrial equipment, and renewable energy power plan.[1, 2] By contrast with traditional capacitors, supercapacitors offer advantages in faster dynamics of charge-discharge, higher power and energy density, longer cyclic life, and lower maintenance. According to the nature of charge storage mechanisms, supercapacitors can be classified into two categories, electrical double layer capacitors (EDLCs) and pseudocapacitors. The former capacitance surface charge separation process based on the electrodes and electrolytes interfaces, while the latter pseudocapacitive process relied on the redox reactions occurred in the electrode materials. Normally, the capacitance of pseudocapacitors is higher than that of EDLCs. However, two kinds of separate capacitor materials generally cannot meet the requirements of supercapacitors. Therefore, it requires a great deal of research effort to improve the capacitive performance of supercapacitors. In order to increase the energy density of supercapacitors, electrode materials with higher active surface area and conductivity which can store both EDLC



Journal of Materials Chemistry A Accepted Manuscript

and pseudocapacitance are required.

Carbon nanomaterials, in particular as electrode materials for supercapacitors have attracted the scientific community in EDLCs. As a typical carbon material, graphene, with a $sp^2$-hybridized carbon atoms packaged into honeycomb lattice structure, is identified as great chemical and thermal stability, high mechanical flexibility, superior electrical conductivity, and large surface area. However, the maximum capacitance is limited by the active electrode surface area and can't meet the requirements as a capacitor. Compared with one dimensional carbon materials, the unique planar structure of graphene makes it easier and more flexible to integrate with metal oxides. Various noble and transition metal oxides such as $MnO_2$, $RuO_2$, NiO, and $SnO_2$ were used as electrode materials of pseudocapacitors.[3, 4, 5, 6] Among these oxides, $MnO_2$, due to its good proton-electron intercalation properties, high specific capacitance, low cost, abundance, and environmental friendly nature, has draw tremendous attention as active electrode material. Nevertheless, the capacitance of $MnO_2$ electrode is restricted by the poor electrical conductivity. Thus, many methods have been taken to eliminate the disadvantage by synthesizing hybrid materials, such as the introduction of conducting carbon materials. The conducting carbon materials can enhance the capacitance because of fast electron transfer during Faradic charge transfer reactions.

The graphene–manganese dioxide composites displayed improved capacitive performance due to the pseudocapacitive properties of $MnO_2$ and high conductivity of graphene. Different morphologies of $MnO_2$ have been anchored on graphene or reduced graphene oxide as electrode materials for supercapacitors through physical mixing or chemical reactions. In the previous reports, various microstructures of graphene/$MnO_2$ nanocomposites, such as graphene/$MnO_2$ nanowires,[7] graphene/flower–like $MnO_2$,[8] graphene/$MnO_2$ rod composites,[9] graphene/$MnO_2$ nanoparticles,[10] reduced graphene oxide/$MnO_2$ nanosheets,[11] and reduced graphene oxide/$MnO_2$ hollow spheres[12] have been reported. The formation of graphene or reduced graphene oxide metal oxide composite can be obtained through a variety of methods, such as hydrothermal process, electrodeposition, co-precipitation,[13] spray pyrolyzing,[14] and so on.

Herein, the functionalized graphene/$MnO_2$ composites were synthesized by making use of the strong electrostatic interactions between them. The functionalized graphene were obtained by changing the surface charge of graphene from negative to positive with poly (diallyldimethylammonium) chloride under sustaining sonication. Scanning electron microscopy (SEM), Fourier transform infrared spectroscopy (FTIR), X-ray photoelectron spectroscopy (XPS), and Powder X-ray diffraction (XRD) were used to study the structure and composition of the graphene/$MnO_2$ composites. Furthermore, from the results of the electrochemical experiments of graphene/$MnO_2$ (flowerlike nanospheres) and graphene/$MnO_2$ (nanowires) composites, the former exhibit larger specific capacitance and faster galvanostatic charge/discharge process than the latter, demonstrating its good capacity to serve as a high-performance supercapacitor electrode material.

## 2. Experimental section

### 2.1 Materials

Graphite flake (natural, −325 mesh, 99.8%) was purchased from Alfa Aesar Chemical Reagent Co. and used for synthesis of graphene oxide (GO). GO, containing a lot of oxygen functional groups, was prepared by the modified Hummers method as described previously.[15] Poly(diallyldimethylammonium) chloride (PDDA, *MW*=200,000–350,000, 20 wt% in water) was

Journal of Materials Chemistry A Accepted Manuscript

purchased from Aladdin Chemistry Co. Ltd. Potassium permanganate ($KMnO_4$), manganese sulfate ($MnSO_4·H_2O$), sodium sulfate ($Na_2SO_4$), acetylene black, polytetrafluorene ethylene (PTFE), and ethanol were purchased from Shanghai Chemical Reagent Co. All chemicals were of analytical grade and used as received without further treatment.

**2.2 Preparation of different morphologies of $MnO_2$**

Different morphologies of $MnO_2$ were obtained by controlling hydrothermal reaction time. The procedure was carried out following the reported procedure with little modification. [16] The detailed steps were as follows: 0.2 g of $MnSO_4·H_2O$ were dissolved in 5 mL of deionized water under stirring. 10 mL aqueous solution containing 0.5 g of $KMnO_4$ was added drop by drop quickly at room temperature. Subsequently, the mixture was stirred adequately for a few minutes, then transferred to a Teflon-lined stainless steel autoclave and loaded into an oven heated to 140 °C for 2 h. The autoclave was cooled to ambient temperature gradually after the given time. The precipitate was centrifuged and washed with deionized water and ethanol several times, and then dried in a vacuum at 60 °C for 12 h and gathered $MnO_2$ flowerlike nanospheres power. As to obtain $MnO_2$ nanowires, the preparation process was same with the above described steps except the dwell time was extended to 12 h.

**2.2 Preparation of functionalized graphene**

The surface oxygen-containing functional groups of GO was removed by hydrothermal treatment method to obtain graphene. In a typical preparation procedure, 10 mg of GO was diluted with 12.5 mL of deionized water under vigorous stirring for 30 min. Then transferred the solution to a Teflon-lined pressure vessel and maintained the temperature at 170 °C for 20 h. After cooling down to room temperature, the resulting suspension was separated by centrifugation and washing with deionzed water. Then the precipitate was redissolved in 10 mL of deionized water under ultrasonication for 30 min. Finally, 15 μl of PDDA was added gradually and formed a homogeneous suspension under sonication for another 30 min. Then the functionalized graphene was received (named as FG). The surface charge of graphene was changed from negative to positive after treatment by PDDA.

**2.4 Preparation of functionalized graphene/$MnO_2$ (flowerlike nanospheres) and graphene/$MnO_2$ (nanowires) composites**

For preparing functionalized graphene/$MnO_2$ composites, $MnO_2$ with different morphologies were anchored on the surfaces and edges of graphene through an electrostatic interaction. 5 mL aqueous solution containing 30 mg of flowerlike $MnO_2$ nanospheres was mixed with 10 mL of functionalized graphene suspension under sonication. After 30 min, the mixture was centrifuged and washed with deionized water and ethanol for several times. Then the resulting precipitate was dried overnight at 60 °C under a vacuum. Then the functionalized graphene/$MnO_2$ (flowerlike nanospheres) composite was collected (donated as FG-f-$MnO_2$). The preparation of functionalized graphene/$MnO_2$ (nanowires) composite followed the same procedures by using equivalent $MnO_2$ nanowires instead of flowerlike $MnO_2$ nanospheres (named as FG-w-$MnO_2$).

**2.3 Preparation of the functionalized graphene/$MnO_2$ composites modified electrodes**

For evaluating the electrochemical properties of graphene/$MnO_2$ composites, a three-electrode configuration was fabricated. The as-prepared graphene/$MnO_2$ composites were mixed with acetylene black and PTFE in the weight ratio of 70:25:5, and then a few drops of ethanol was added to form suspension. Then the slurry were pressed onto graphite electrodes as working electrodes and dried in vacuum at 80 °C for 12 h. The mass loading of active materials in the



Journal of Materials Chemistry A Accepted Manuscript

electrode was about 9 mg·cm$^{-2}$. The thickness of the working electrodes was measured to be around 60 um. The active materials exists ohmic resistance that will produce ohms voltage drop to affect the capacitance of capacitor. The thicker electrode will generate larger ohmic resistance. The electrode with a thickness of 60 um showed the best capacitance performance in this work. In addition, saturated calomel and platinum wire electrodes were used as the reference and counter electrodes, respectively. An aqueous solution of 1.0 M $Na_2SO_4$ was acted as the electrolyte.

**2.4 Characterization**

The morphologies of the functionalized graphene/$MnO_2$ composites were examined by scanning electron microscopy (SEM, S4800). FT-IR spectra of products in KBr pellets were recorded using a Bruker model VECTOR22 Fourier transform spectrometer. X-ray photoelectron spectroscopic (XPS) measurements were preceded on ESCA-LAB MK II X-ray photoelectron spectrometer. Power X-ray diffraction (XRD) patterns of samples were detected using Philip XRD X'PERT PRO diffractometer with Cu Kα X-ray radiation. To test the electrochemical properties of the samples, a classical three-electrode cell was used on a CHI 660C electrochemical workstation (Chenhua, Shanghai). The electrochemical behaviors of the supercapacitor systems were estimated by cyclic voltammograms (CV) and galvanostatic charge/discharge. All the amperometric experiments were manipulated with the potential windows of 0.1-1.1 V in a 1.0 M $Na_2SO_4$ electrolyte.

**3. Results and Discussion**

Sonochemistry methods have been successfully used for preparation of various metal oxides nanostructures at room temperature, ambient pressure, and short reaction time.[17] In this work, different morphologies of functionalized graphene/$MnO_2$ composites were synthesized by ultrasonic self-assembly method, which could prevent graphene from restacking. $MnO_2$ with two different shapes was prepared by controlling the hydrothermal reaction time. The hydrothermal technique includes management the reaction to a temperature generally between 100 and 200 $^{\circ}$C under auto-generated pressure in a closed vessel. Due to the variation in the properties of water with diversification in time, the reactive conditions are significant to determine the properties of the products. [18] When hydrothermal treated for 2 h at 140 $^{\circ}$C, the size of individual whisker would be increased resulting in the formation of flower-like morphology. With the hydrothermal reaction time increased, the bulk agglomerated nanowhiskers showed an increase in density and leaned to loosen leading to the formation of nanowire structure. Although GO was treated with hydrothermal and ultrasonic reduction, there were still some functional groups containing oxygen. The presence of oxygen-containing functional groups on the surfaces and edges of the GO nanosheet leads to its negatively charged nature. [19] The surface of graphene was positively charged after reaction with PDDA. By taking advantage of the strong electrostatic interactions between negatively charged $MnO_2$ and positively charged graphene, the graphene/$MnO_2$ composites with different morphologies could be obtained. Several advantages could be provided by using the functionalization of graphene, such as the improvement of hydrophilic property of graphene, transfer the surface charge from negatively to positively nature, and prevent graphene from restacking after reduction for the loss in surface oxygen-containing groups.[20]

Fig. 1 presents the typical SEM images of the obtained FG-f-$MnO_2$ (a) and FG-w-$MnO_2$ (b) composites. As observed, the different shapes of $MnO_2$ were densely dispersed on the surfaces and edges of graphene nanosheets uniformly. In addition, the diameters of the as-prepared $MnO_2$



Journal of Materials Chemistry A Accepted Manuscript

nanowires vary from 50 to 100 nm with an average length up to 3-6 μm. The diameter of $MnO_2$ flowerlike nanospheres is about 500 nm. As we could see from the pictures, different morphologies of $MnO_2$ uniformly anchored on graphene, which had a direct effect on the electrochemical properties of the materials.

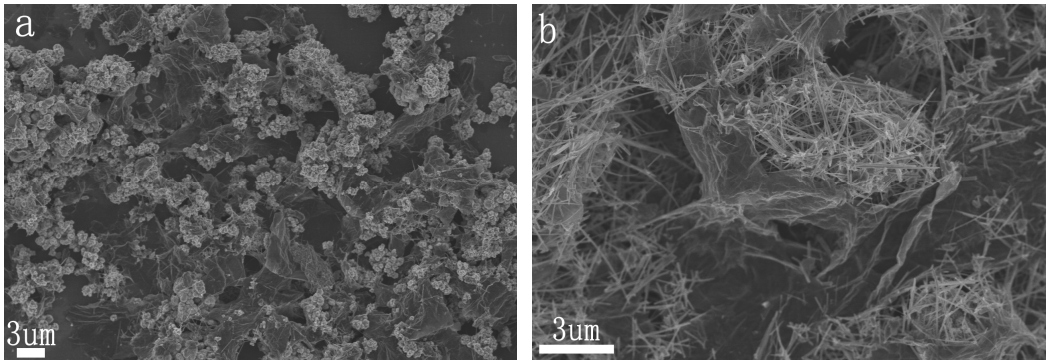


Fig. 1 SEM images of FG-f-$MnO_2$ (a) and FG-w-$MnO_2$ (b).

Fig. 2 gives FT-IR spectra of GO and graphene/$MnO_2$ composites. It clearly shows that the characteristic peak around at 1727 $cm^{-1}$ in the spectrum of GO is associated with vibration of the C=O bond of carboxylic groups. In addition, the absorption peak centered at 1620 $cm^{-1}$ can be attributed to the residual water molecules and the stretching skeletal of aromatic C=C domains. The vibration of O=C-O from carboxylate is appeared at about 1387 $cm^{-1}$, the bands stretching vibrations at 1225 and 1051 $cm^{-1}$ correspond to epoxy and alkoxy C–O groups, respectively.[21, 22] Since the existence of oxygen-containing functional groups, GO surfaces and edges load negative charge, which is consistent with the previous literature.[15] By contrast, the spectra of graphene/$MnO_2$ composites differ from that of GO. The intensities of absorption peaks of GO decreased dramatically, showing the reduction of GO in the composites. Additionally, a peak about at 520 $cm^{-1}$ is related to Mn-O of structure of $MnO_2$.[23] These results clearly confirmed that the oxygen functionalities groups were removed during hydrothermal process combined with ultrasound technology and graphene/$MnO_2$ composites were successfully synthesized.

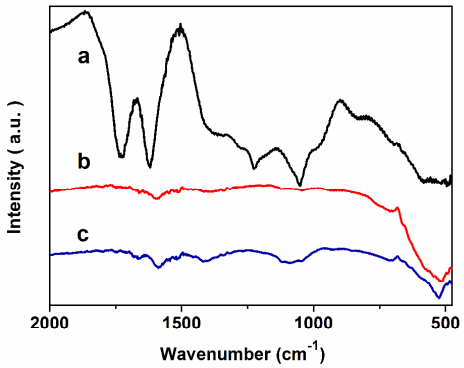


Fig. 2 FTIR spectra of GO (a), FG-f-$MnO_2$ (b), and FG-w-$MnO_2$ (c).

The surface conditions of GO and graphene/$MnO_2$ nanocomposites were further analyzed by



Journal of Materials Chemistry A Accepted Manuscript

XPS. The wide scan survey spectra by XPS were presented in Fig. 3 (A). In the spectrum of GO, there were only two elements, C and O, respectively. However, the signals of elements C, O, and Mn ($2p^{3/2}$, $2p^{1/2}$) could be seen in the composites indicating the formation of graphene/$MnO_2$ composites. Fig. 3 (B) presented the C 1s spectra of GO and graphene/$MnO_2$ nanocomposites, respectively. The XPS spectrum of C 1s of GO can be deconvoluted into four peaks, C-C (284.5 eV), C-O (286.4 eV), C=O (287.0 eV), and O=C-OH (288.4 eV), separately, which was in well agreement with the reported results.[24] Compared with C 1s spectra of GO, that of graphene/$MnO_2$ nanocomposites (Fig. 3b and 3c) showed strong binding energy peaks of the carbon bonds at 284.3 and 283.9 eV, respectively. In contrast, the peak intensity of C-O and C=O/O=C-OH in graphene/$MnO_2$ tremendously decreased after the hydrothermal and ultrasonic processes, indicating the successful formation of graphene in composites.[20]

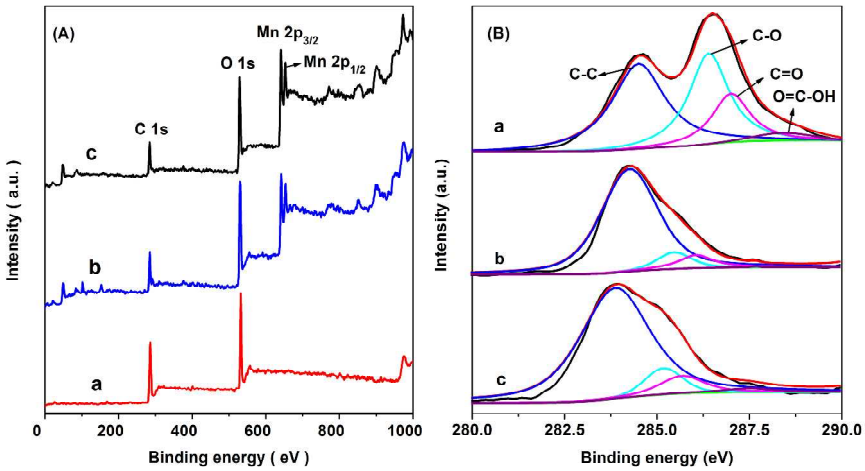


Fig. 3 (A) XPS spectra of GO (a), FG-w-$MnO_2$ (b), and FG-f-$MnO_2$ (c); (B) XPS data of the C1s regions of GO (a), FG-w-$MnO_2$ (b), and FG-f-$MnO_2$ (c).

The crystal structure of the samples was analyzed by XRD. Fig. 4 shows the obtained diffraction patterns of the as-prepared $MnO_2$ and graphene/$MnO_2$ composites. In general, all the reflections can be readily indexed to a pure tetragonal phase of α-$MnO_2$ (ICDD-JCPDS No. 44-0141) .[16] The broad peaks centered at about 12.4˚, 18.0˚, 28.6˚, 37.5˚, and 49.7˚ can be indexed to (110), (200), (310), (211), and (411), respectively.[25] As shown in the figure, the peaks of $MnO_2$ and graphene/$MnO_2$ composites were almost appeared at the same location. However, the peaks of $MnO_2$ nanowires and FG-w-$MnO_2$ displayed at round 37.5˚ were stronger than the same position of $MnO_2$ flowerlike nanospheres and FG-f-$MnO_2$ showing that the crystalline of $MnO_2$ nanowires is higher than that of $MnO_2$ flowerlike nanospheres. The reason is probably that there is an increase in crystalline with respect to the increase of hydrothermal dwell time from 2 h to 12 h. With the reaction time increased, the crystalline is increased.[18]

Journal of Materials Chemistry A Accepted Manuscript

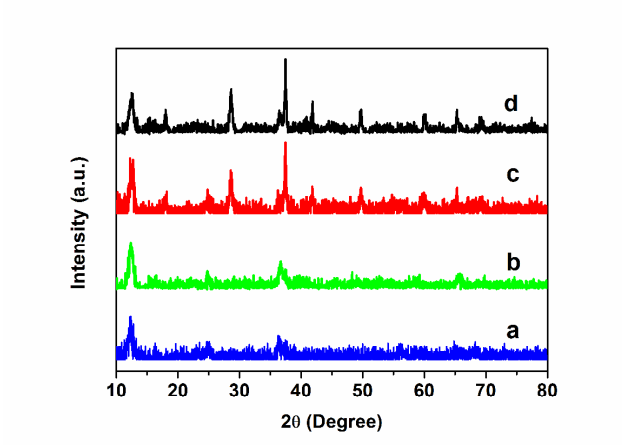


Fig. 4 XRD patterns of flowerlike $MnO_2$ (a), FG-f-$MnO_2$ (b), nanowire $MnO_2$ (c), and FG-w-$MnO_2$ (d).

To evaluate the electrochemical performance of the supercapacitor based on graphene/$MnO_2$ with different shapes, cyclic voltammetry (CV) and galvanostatic charge/discharge were employed. Fig. 5 (A) shows the CV curves of as-prepared FG-w-$MnO_2$ and FG-f-$MnO_2$ based on the three-electrode configuration at a scan rate of 100 mV $s^{-1}$ in 1 M $Na_2SO_4$ solution in the potential range between 0.1 and 1.1 V (vs. SCE). Both of the CV curves reveal almost rectangle-like shapes without obvious redox peaks, indicating ideal capacitive behavior and symmetric characteristics of a supercapacitor.[26] The fast and reversible successive surface redox reactions define the behavior of the voltammogram, whose shape is close to that of the EDLC, which shows the successive multiple surface redox reactions leading to the pseudo-capacitive charge storage mechanism. A part of the current is greater than zero is related to the oxidation from Mn (III) to Mn (IV), on the contrary, the part of the current is less than zero part refers to the reduction from Mn (IV) to Mn (III).[36] It can be easily seen from the figure that FG-f-$MnO_2$ shows larger enclosed area than that of FG-w-$MnO_2$. The galvanostatic charge/discharge curves of FG-w-$MnO_2$ (a) and FG-f-$MnO_2$ (b) at 1.0 A $g^{-1}$ are shown in Fig. 5 (B). The specific capacitances are 310 and 408 F $g^{-1}$ of FG-w-$MnO_2$ and FG-f-$MnO_2$, respectively. The results show that FG-f-$MnO_2$ possesses superior capacitive properties to FG-w-$MnO_2$ composite. As a model, further tests of FG-f-$MnO_2$ composite were also included here with the object of application to the supercapacitor electrode material.

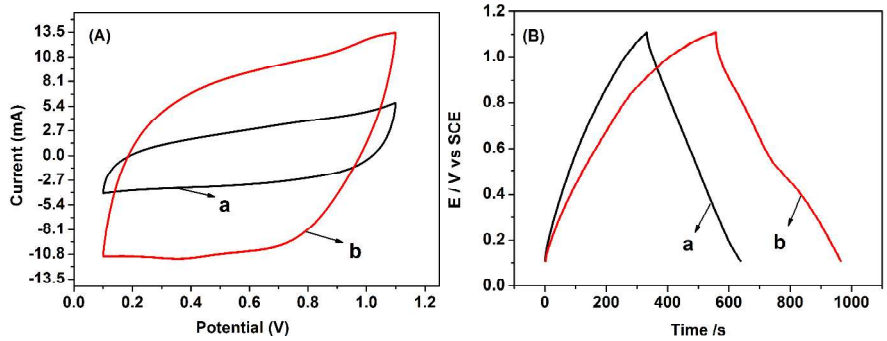


Fig. 5 (A) Cyclic voltammograms of FG-w-$MnO_2$ (a) and FG-f-$MnO_2$ (b) at 100 mV $s^{-1}$ scan rate; (B) Galvanostatic charge/discharge curves of the FG-w-$MnO_2$ (a) and FG-f-$MnO_2$ (b) at current



Journal of Materials Chemistry A Accepted Manuscript

density of 1.0 A $g^{-1}$ with potential windows of 0.1-1.1 V in 1 M $Na_2SO_4$.

Fig. 6 (a) shows CV curves of the FG-f-$MnO_2$ composite at different scan rates of 2, 5, 10, 25, 50, 75, and 100 mV $s^{-1}$ with potential windows between 0.1 to 1.1 V in 1M $Na_2SO_4$ aqueous solution. The quasi-rectangle of CV curves at different scan rates indicated the fast charging/discharging processes and excellent behaviors in the supercapacitor electrodes.[27, 28] Meanwhile, the curve shape is gradually deformed from rectangular with the scan rate increased, for the reason of internal resistance and pseudocapacitance of the composites electrode.[29, 30] The shape of FG-f-$MnO_2$ curve is nearly rectangular at 2 mV $s^{-1}$, demonstrating the presence of electrical double-layer capacitance and pseudocapacitance.[31] As the scan rate increasing, the curve symmetry becomes weaken, showing its EDLC and pseudocapacitance properties. The formula for calculating the specific capacitance can be described as follows: [23]

$$Cg = (\int IdV) \Big/ (mVv) \quad (2)$$

Where $I$ represents the response current density (A/g), $V$ is the potential window (V), $v$ is the potential scan rate (mV $s^{-1}$), and $m$ is the mass of the active material in the electrode (g). The specific capacitance is 405, 364, 338, 294, 250, 225, and 206 F $g^{-1}$ at the scan rates of 2, 5, 10, 25, 50, 75, and 100 mV $s^{-1}$, respectively. The electrolyte ion cannot contact with the surface and internal of active electrode fully at high scan rate. Thus, with the increase of the scan rate, the rapid movement of the electrolyte ions in contact with the active electrode leads to the decrease of the specific capacitance.

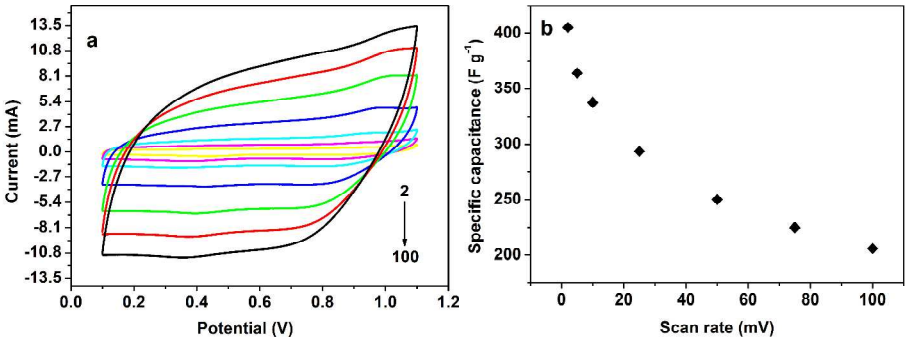


Fig. 6 (a) Cyclic voltammograms of FG-f-$MnO_2$ at different scan rates from inner to outside (2, 5, 10, 25, 50, 75, and 100 mV $s^{-1}$), respectively; (b) Specific capacitance of FG-f-$MnO_2$ at different scan rates.

To assess more performance about FG-f-$MnO_2$ composite as electrode material for supercapacitor, galvanostatic charge/discharge measurements were conducted. The specific capacitances of FG-f-$MnO_2$ nanocomposites at different current densities in 1 M $Na_2SO_4$ at the voltage window of 0.1 - 1.1 V are shown in Fig.7 (A). The corresponding specific capacitance of FG-f-$MnO_2$ composite is 514, 465, 430, 417, and 408 F $g^{-1}$ at different current densities of 0.2, 0.4, 0.6, 0.8, and 1.0 A $g^{-1}$, respectively. Compared with the theoretical value of $MnO_2$ (1370 F/g), the calculated capacitance (514 F/g) is lost. As we known, only the $MnO_2$ surface is contributed to the pseudocapacitive behavior of $MnO_2$. And the larger size of $MnO_2$ nanoparticles also led to the low capacitance.[35] In addition, another possible reason might be due to that the combination of graphene with low specific capacitance. In the charge/discharge process, the discharge curve with



Journal of Materials Chemistry A Accepted Manuscript

a slight curvature is almost symmetrical to charge corresponding counterpart, indicating good reversibility of mixed materials.[32] Fig.7 (B) shows different current densities corresponding to different values of the specific capacitance. It can be seen that with the current density increases, the value of specific capacitance decreases. The high discharge current density leads to electrolyte ions can not enter the internal structure of the electro-active material.[33]

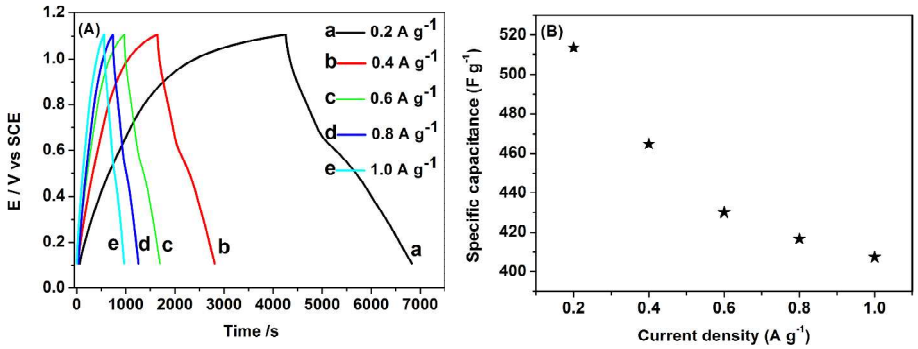


Fig. 7 Galvanostatic charge/discharge
(A) and Specific capacitance (B) of FG-f-$MnO_2$ in 1.0 M $Na_2SO_4$ at different current densities of 0.2, 0.4, 0.6, 0.8, and 1.0 A $g^{-1}$, respectively.

Long cycle life of supercapacitor is very important for its practical applications. The electrochemical stability of the FG-f-$MnO_2$ nanocomposite in 1 M $Na_2SO_4$ electrolyte solution has been further tested by galvanostatic charge/discharge over the potential window of 0.1−1.1 V. As shown in Fig. 8, the specific capacitance of the FG-f-$MnO_2$ composite electrodes still remains above 367 F $g^{-1}$ at a current density of 1 A $g^{-1}$ after 1000 cycles (about 90 % of the original value). The main reason for capacitance decrease is the active material dissolving in the electrolyte solution.[34] These results illustrates that the FG-f-$MnO_2$ composite possesses good cycling stability and long lifetime. Additionally, the reproducibility of the FG-f-$MnO_2$-based supercapacitor was investigated by successively testing 4 times, the relative standard deviation (RSD) was 1.5 %, demonstrating a good reproducibility.

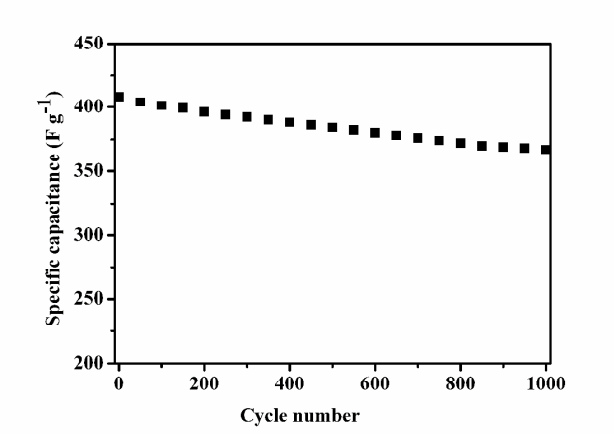


Fig. 8 The specific capacitance changes of FG-f-$MnO_2$ at a constant current density of 1.0 A $g^{-1}$ as a function of cycle number.

## 4. Conclusion



Journal of Materials Chemistry A Accepted Manuscript

Functionalized graphene/$MnO_2$ composites with different shapes are synthesized by ultrasonic self-assembly method with the treatment of PDDA. The as-prepared products were characterized by X-ray diffraction, scanning electron microscopy, X-ray photoelectron spectroscopic, and Fourier transform infrared spectroscopy. Furthermore, the electrochemical properties of the composites were investigated by cyclic voltammetry and galvanostatic charge-discharge measurements. The synergistic effect between high conductivity of graphene and pseudo capacitive of $MnO_2$ generates large capacitance of composites. The FG-f-$MnO_2$ composite exhibits a considerable specific capacitance of 514 F $g^{-1}$ at a current density of 0.2 A $g^{-1}$ in 1 M $Na_2SO_4$ aqueous solution and good long-term cycle stability, indicating its potential application as a remarkable electrode material for high-performance supercapacitors.

**Acknowledgment** This work is supported by the National Natural Science Foundation of China (Nos. 20905038, 20903057, 21105050, and 21005040), National Basic Research Program of China (Nos. 2009CB930600, 2012CB933301), Research Found for the Doctoral Program of Higher Education of China (20113223120004), and the Ministry of Education of China (No. IRT1148).

## References

1 U. Eberle and R. von Helmolt, *Energy Environ. Sci.*, 2010, **3**, 689-699.
2 J. Zhang and X. S. Zhao, *Chemsuschem*, 2012, **5**, 818-841.
3 X. Feng, Z. Yan, N. Chen, Y. Zhang, Y. Ma, X. Liu, Q. Fan, L. Wang and W. Huang, *J. Mater.Chem. A*, 2013, **1**, 12818-12825.
4 Z. S. Wu, D. W. Wang, W. Ren, J. Zhao, G. Zhou, F. Li and H. M. Cheng, *Adv. Funct. Mater.* , 2010, **20**, 3595-3602.
5 X. H. Xia, J. P. Tu, Y. J. Mai, R. Chen, X. L. Wang, C. D. Gu and X. B. Zhao, *Chem. - Eur. J.*, 2011, **17**, 10898-10905.
6 F. H. Li, J. F. Song, H. F. Yang, S. Y. Gan, Q. X. Zhang, D. X. Han, A. Ivaska and L. Niu, *Nanotechnology*, 2009, **20**.
7 S. Chen, J. Zhu, X. Wu, Q. Han and X. Wang, *Acs Nano*, 2010, **4**, 2822-2830.
8 L. Mao, K. Zhang, H. S. O. Chan and J. Wu, *J. Mater. Chem.*, 2012, **22**, 1845-1851.
9 M.-T. Lee, C.-Y. Fan, Y.-C. Wang, H.-Y. Li, J.-K. Chang and C.-M. Tseng, *J. Mater. Chem. A*, 2013, **1**, 3395-3405.
10 C. Chen, W. Fu and C. Yu, *Mater. Lett.* , 2012, **82**, 133-136.
11 R. S. Kalubarme, C.-H. Ahn and C.-J. Park, *Scripta Mater*, 2013, **68**, 619-622.
12 Y. Qian, S. Lu and F. Gao, *J. Mater. Chem.*, 2011, **46**, 3517-3522.
13 L. Peng, X. Peng, B. Liu, C. Wu, Y. Xie and G. Yu, *Nano Lett*, 2013, **13**, 2151-2157.
14 A. Chidembo, S. H. Aboutalebi, K. Konstantinov, M. Salari, B. Winton, S. A. Yamini, I. P. Nevirkovets and H. K. Liu, *Energy Environ. Sci.*, 2012, **5**, 5236-5240.
15 X.-M. Feng, R.-M. Li, Y.-W. Ma, R.-F. Chen, N.-E. Shi, Q.-L. Fan and W. Huang, *Adv. Funct. Mater.* , 2011, **21**, 2989-2996.
16 F. Cheng, Y. Su, J. Liang, Z. Tao and J. Chen, *Chem. Mater.*, 2010, **22**, 898-905.
17 A. Zolfaghari, H. R. Naderi and H. R. Mortaheb, *J. Electroanal. Chem.*, 2013, **697**, 60-67.
18 P. K. Nayak and N. Munichandraiah, *J. Solid State Electrochem.* , 2012, **16**, 2739-2749.

Journal of Materials Chemistry A Accepted Manuscript

19 Z.-S. Wu, W. Ren, D.-W. Wang, F. Li, B. Liu and H.-M. Cheng, *Acs Nano*, 2010, **4**, 5835-5842.
20 J. Zhang, J. Jiang and X. S. Zhao, *J. Phys. Chem. C*, 2011, **115**, 6448-6454.
21 S. Sheshmani and R. Amini, *Carbohydr. Polym.*, 2013, **95**, 348-359.
22 Y. Li, N. Zhao, C. Shi, E. Liu and C. He, *J. Phys. Chem. C*, 2012, **116**, 25226-25232.
23 J. Zhu and J. He, *ACS Appl. Mat. Interfaces*, 2012, **4**, 1770-1776.
24 D. R. Dreyer, S. Park, C. W. Bielawski and R. S. Ruoff, *Chem. Soc. Rev.*, 2010, **39**, 228-240.
25 Y. Yu, B. Zhang, Y.-B. He, Z.-D. Huang, S.-W. Oh and J.-K. Kim, *J. Phys. Chem. A*, 2013, **1**, 1163-1170.
26 X. Wang, H. Liu, X. Chen, D. G. Evans and W. Yang, *Electrochim Acta*, 2012, **78**, 115-121.
27 M. D. Stoller, S. Park, Y. Zhu, J. An and R. S. Ruoff, *Nano Lett*, 2008, **8**, 3498-3502.
28 M. Zhi, C. Xiang, J. Li, M. Li and N. Wu, *Nanoscale*, 2013, **5**, 72-88.
29 Y. Wang, Z. Shi, Y. Huang, Y. Ma, C. Wang, M. Chen and Y. Chen, *J. Phys. Chem. C*, 2009, **113**, 13103-13107.
30 Y.-L. Chen, Z.-A. Hu, Y.-Q. Chang, H.-W. Wang, Z.-Y. Zhang, Y.-Y. Yang and H.-Y. Wu, *J. Phys. Chem. C*, 2011, **115**, 2563-2571.
31 G. Xiong, K. P. S. S. Hembram, R. G. Reifenberger and T. S. Fisher, *J. Power Sources* 2013, **227**, 254-259.
32 S. Chen, J. Zhu and X. Wang, *Acs Nano*, 2010, **4**, 6212-6218.
33 Z. Fan, J. Yan, T. Wei, L. Zhi, G. Ning, T. Li and F. Wei, *Adv. Funct. Mater. ,* 2011, **21**, 2366-2375.
34 J.-K. Chang, M.-T. Lee, C.-H. Huang, and W.-T. Tsai, *Mater. Chem. Phys.,* 2008, **108**, 124-131.
35 X.-P. Dong, W.-H. Shen, J.-L. Gu, L.-M. Xiong, Y.-F. Zhu, H. Li, and J.-L. Shi, *J. Phys. Chem. B*, 2006, 110, 6015-6019
36 P. Simon, and Y. Gogotsi, *Nat. Mater.,* 2008*,* 7, 845-854.

Journal of Materials Chemistry A Accepted Manuscript